




Research Article

Modeling and Optimization of Electrodeposition Process for Copper Nanoparticle Synthesis Using ANN and Nature-Inspired Algorithms

A. Tamilvanan,¹ K. Balamurugan ,² T. Mohanraj ,³ and Yesgat Admassu ⁴

¹Department of Mechanical Engineering, Kongu Engineering College, Erode-638060, India

²Department of Mechanical Engineering, Government College of Engineering-Erode, (Formerly IRTT), Erode-638316, India

³Department of Mechanical Engineering, Amrita School of Engineering, Amrita Vishwa Vidyapeetham, Coimbatore, India

⁴Institute of Research Development, Defence University, Bishoftu, Ethiopia

Correspondence should be addressed to Yesgat Admassu; yesgat.admassu@dec.edu.et

Received 27 October 2022; Revised 22 May 2023; Accepted 21 June 2023; Published 7 July 2023

Academic Editor: Leander Tapfer

Copyright © 2023 A. Tamilvanan et al. This is an open access article distributed under the Creative Commons Attribution License, which permits unrestricted use, distribution, and reproduction in any medium, provided the original work is properly cited.

Due to its outstanding physical, chemical, and thermal properties, an increasing consideration has been paid to produce copper (Cu) nanoparticles (NPs). Various methods are accessible for producing Cu NPs by conceiving the top-down and bottom-up approaches. Electrodeposition is a bottom-up method to synthesize high-quality Cu NPs at a low cost. The attributes of Cu NPs rely on their way of deduction and electrochemical process parameters. This work aims to deduce the mean size of Cu NPs. Artificial neural networks (ANN) and nature-inspired algorithms, namely genetic algorithm (GA), firefly algorithm (FA), and cuckoo search (CS) algorithm were used to predict and optimize the electrochemical parameters. The results obtained from ANN prediction agreed with data from the electrodeposition process. All nature-inspired algorithms reveal similar operating conditions as optimal parameters. The minimum NP size of 20 nm was obtained for the process parameters of $4 \text{ g}\cdot\text{l}^{-1}$ of CuSO_4 concentration, electrode distance of 3 cm, and a potential difference of 27 V. The synthesized NP size was in line with the anticipated NP size. The scanning electron microscope and X-ray diffractometer (XRD) were performed to analyze the nanoparticle size and morphology.

1. Introduction

Currently, nanotechnology has attracted researchers in various fields. The attributes of materials, particles, and molecules available in smaller sizes change dramatically at nanoscale particles. Nanotechnology is the engineering system that functions at the scale of a Nanometer (10^{-9} m). Copper (Cu) is one of the most popular and expensive metals employed in engineering applications owing to its electrical, catalytic, and thermal properties among the various materials [1]. Cu nanoparticles (NPs) have been recognized due to their enhanced electrical and thermal conductivity, higher melting point, outstanding solderability, low electrochemical migration performance, and low cost [2]. The preparation of Cu NPs is incredibly intricate compared to other gracious metals like Au, Ag, and Pt.

The production of NPs has been categorized as top-down and bottom-up approaches [3]. Various techniques to

synthesize Cu NPs include microemulsion, polyol process, chemical reduction [4], electrochemical, sonochemical reduction, hydrothermal, microwave methods, biological synthesis, sol-gel synthesis, mechanical milling, laser excision, vapor phase synthesis, and pulsed wire discharge [5]. With these approaches, electrochemical is the most suitable for synthesizing Cu NPs because of its easy operation, high flexibility, less contamination, and readily available equipment. It does not require vacuum systems to synthesize the uncontaminated product [6, 7]. Electrodeposition is a nonvacuum electrochemical method highly desirable to thin film deposition due to its ability to deposit component alloys at room temperature, making it cheaper and economical. In this method, the deposition of thin metallic films is done onto the substrate by reducing cations without any unwanted reactions. Also, the electrodeposition process has the advantage of low-cost and large-area semiconductor growth techniques for

applications in the macroelectronic devices such as solar panels and large-area display devices [8]. Cu NPs have gained more interest in heat transfer, additives, inkjet printing, biomedical applications, catalytic synthesis, and so on. Adding Cu NPs as a fuel additive significantly improves the characteristics of diesel and biodiesel fuels [9].

Electrodeposition is a well-proven method with advantages like deposition rate and yield, which can be effortlessly regulated by varying the electrodeposition parameters. The achievable deposition rate in the electrodeposition process is 0.025–1.23 mg/min [10]. It is a simple method for synthesizing homogeneously dispersed electrocatalysts without added capping agents. Also, it is expandable under surrounding conditions and permits controlled, and faceted nanocrystal structure development [11].

Many researchers have focused on electrodeposition from acidified sulphate by galvanostatic and potentiostatic methods [6, 7, 11]. According to their reports, the particle size, growth, morphology, chemical constitution, and other properties of Cu NPs mainly depend on the synthesis parameters like electrolyte concentration, the distance between electrodes, the type of anode, temperature, current density, the quantity of evolved hydrogen, and removal time of NPs. The preparation of Cu NPs comprises of formation of a nucleus and augmentation. Cu NPs size can be controlled by varying the proportional rate of nucleus formation and enlargement through preservatives [12]. Polyvinylpyrrolidone is one of the most effective organic preservatives utilized in the electrodeposition process to synthesize the Cu NPs size [13]. The electrolysis of Sn was prepared through bimetallic electrode [14]. Crespo [15] performed a detailed review of various methods of electrodeposition. Aluminium was deposited on the platinum substrate with potentiostatic, galvanostatic, monopolar, and bipolar current pulse polarization methods. The authors found that the adhesive strength of deposited aluminium was significantly enhanced using bipolar current pulse polarization due to its anodic and cathodic pulse combination for electrodeposition [16]. The pulse current polarization method is suitable for the deposition of aluminium, and the deposition structure can be controlled by varying the pulse parameters [17].

Numerous conventional and metaheuristic approaches have been applied to solve the nonlinear problem. An artificial neural network (ANN) is a data processing pattern composed of algebraic equations. The ANN data processing units are prepared in three layers: input, hidden, and output. The data are normalized and fed to the input layer of the ANN. The behavior of the hidden layer is decided based on the actions of the input layer and the weights between the input and hidden layer. The output layer's performance relies on the hidden layer's activities and weights between the hidden and output layer. The transfer function specifies the association between input, hidden, and output layers. ANN is a computer model corresponding to the human brain's acquisition of knowledge and decision-making skills [18].

The structure of ANN consists of several interlinked processing units, generally called neurons. The neurons are connected by two or more (input, hidden, and output) and interact

through weights [19]. Nature and influencing strength between interconnected neurons are determined based on scalar weights. Every neuron is associated with all other neurons in the subsequent layer. ANN was used to predict the mean Cu particle size. ANN is a familiar tool in the artificial intelligence approach used to solve complex problems and time-consuming learning processes, reduce computational complexity, and achieve a robust and accurate model. They provide the relationship between the input and output of the system. ANN is used in extensive robotics, forecasting, control, pattern recognition, manufacturing, signal processing, power systems, and optimization. So far, few research works have focused on employing ANN to synthesize Cu NPs.

The use of metaheuristic algorithms like genetic algorithm (GA), simulated annealing (SA), particle swarm optimization (PSO) [20], tabu search (TS), and evolutionary programming (EP) has received considerable attention in various problem domains for optimizing the process parameters. GA is a global optimization tool that removes most deficiencies produced by local searching methods [21]. From the literature, it was found that electrodeposition process parameters are not optimized with nature-inspired algorithms and predict the particle size using the prediction model. This work applies nature-inspired algorithms like GA, FA, and CS algorithms to optimize the process to obtain the optimum parameters to produce Cu NPs. ANN is one of the simple models to predict the particle size of Cu NPs.

2. Background Models

2.1. Optimization Using Genetic Algorithm. A GA is a population-based search algorithm that employs the survival of the fittest. GA is a combinatorial optimization technique developed based on Darwin's theory of evolution and the perception of expected selection and genetics. GA approach comprises three operators, namely selection, crossover, and mutation. GA usually starts with a set of solutions to the problem; the solution set (which acts as chromosomes) is the population. Crossover operation is used to attain a new answer by combining dissimilar chromosomes to generate new, better offspring, and a new solution by varying existing members of the population; this operation is called mutation. The framework of GA is shown in Figure 1. A random initial population is generated. The fitness value of each chromosome is calculated. According to the fitness value, one set of chromosomes is carefully chosen from the initial population.

2.2. Optimization Using Firefly Algorithm. The FA is the most popular swarm intelligence algorithm for optimization-related problems. FA can be applied to optimize the problems of several areas successfully [23]. The application of FA in the electrodeposition process has rarely been found in the literature. Exploration and exploitation are the two most essential stabilizing factors in FA. Exploration is obtaining a distinct range of solutions within a search space. Exploitation searches for the best available exposure while aiming or using the realized data. Fireflies have a flashlight to entice likely mates and warn of potential threats. When the fireflies' distance increases, the flashlight's intensity decreases, and the

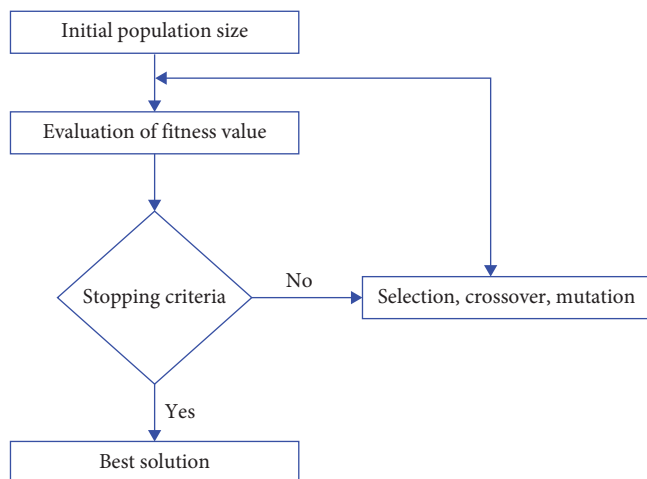


FIGURE 1: Framework of GA [22].

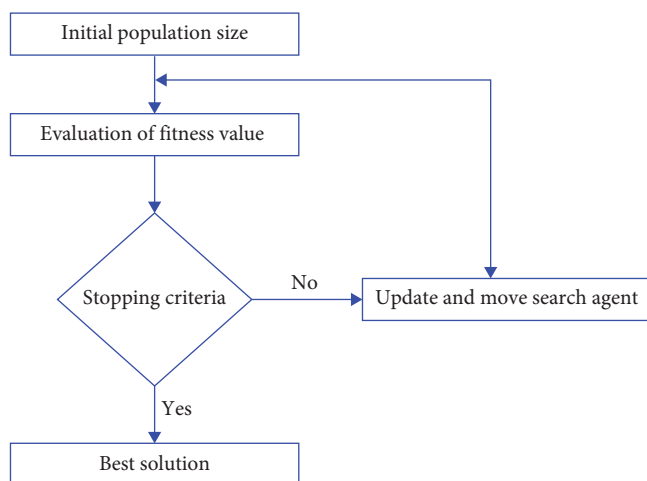


FIGURE 2: Framework of FA [23].

firefly blinks its flashlight at regular instances. The framework of FA is given in Figure 2.

2.3. Optimization Using the Cuckoo Search Algorithm. The CS algorithm is based on cuckoo birds' reproduction method for increasing its inhabitants [24]. Cuckoos are a house of birds with an absolute generative strategy and fast-growing than any other kind. Lévy flights are arbitrary walks, and their walk lengths result from the dissemination of Lévy. The framework of the CS algorithm is shown in Figure 3. The CS algorithm has its own rules for functioning [24].

3. Basics of Electrodeposition

The electrodeposition process is used as an effective method to synthesize various nanomaterials. Electrodeposition is a low-cost method and provides the deposition of pure nanomaterials. The electrodeposition process is a significant process for synthesizing nanomaterials. Electrodeposition process parameters regulate the morphology and rate of deposition on the target surfaces. This process does not

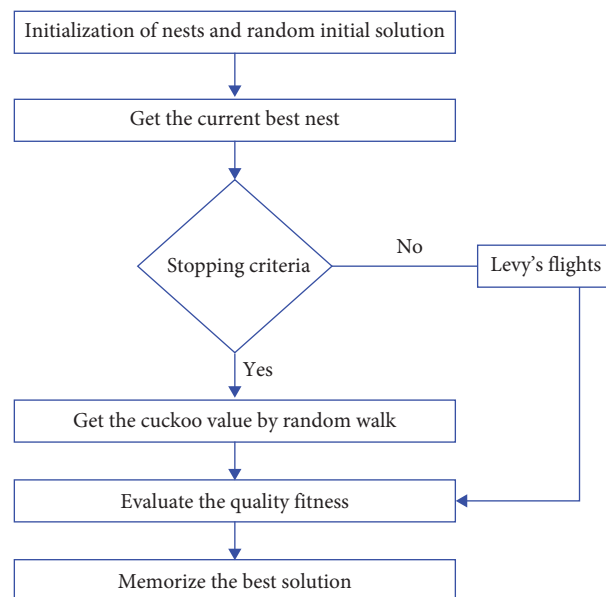


FIGURE 3: Framework of CS algorithm.

require surface-active agents, which streamlines the process for real-world applications. Typically, two metal electrodes (anode and cathode) are submerged in the specialized electrolyte solution [11]. The direct current (DC) source is superficially applied to the electrodes to deposit the target metal on the working electrode (cathode). The deposition thickness is monitored by adjusting the voltage difference between the electrodes (V) and the current density (A). Usually, DC power (in the mW range) was applied to the electrodes, and the positive ions shifted in the direction of the cathode. The electrolyte includes a specific material that controls the electrodeposition process.

4. Experimentation

The electrodeposition process synthesized the Cu NPs from aqueous copper sulfate (CuSO_4) solution. Cu NP electrodeposition was conducted in the electrolyte solution poured in a 500 ml beaker at a constant current of 5 A [6]. This process consists of two pure surfaces (cathode and anode) electrodes placed inside an aqueous solution of CuSO_4 . A homogeneous CuSO_4 acts as an electrolyte. A chemical reaction occurs when Cu electrodes are connected to the power source. A 500 ml electrolyte was prepared for each run by dissolving CuSO_4 salt using distilled water in an electrolytic cell. A cylindrical Cu rod (cathode) was connected to the negative terminal, and a Cu plate was connected to the power supply's positive terminal. The constant current supplied to the electrolytic solution through surface electrodes carried out the electrolysis process.

Figure 4 shows the electrodeposition process to synthesize the Cu NPs. In the electrolysis process, Cu NPs were detached from the copper plate and attached to the copper rod due to the passage of the electrical supply. Cu NPs were detached from the electrode at the end of the electrodeposition process. Cu NPs were washed away numerous times with purified water and then dried in an oven for about 30 min.

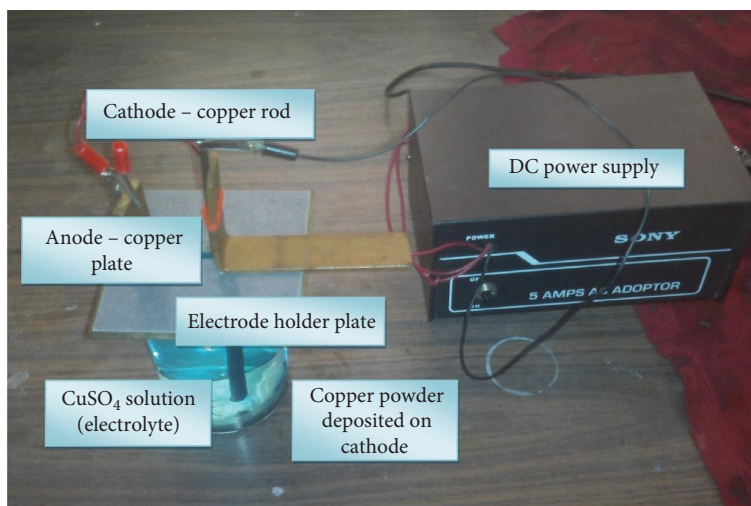


FIGURE 4: Synthesize Cu NPs through the electrodeposition process.



FIGURE 5: Cu NPs deduced through the electrodeposition process.

The Cu NPs synthesized from the electrochemical method were very fine NPs, as shown in Figure 5. The characterization results confirmed that ultrafine powders were Cu NPs. The synthesized Cu NPs were analyzed through a scanning electron microscope (SEM).

4.1. Mean Particle Size of Cu NPs. The properties of Cu NPs are determined by their electrodeposition parameters like electrolyte concentration, the distance between the electrodes, type of anode, temperature, current, the quantity of evolved hydrogen, and removal time of NPs. From the above process parameters, three reference parameters, namely electrolyte concentration, the distance between the electrodes, and the potential difference among electrodes were selected for this work. The preferred process parameters were used to carry out the experiments. Experiments were devised using response surface methodology (RSM) central composite design (CCD) ($\alpha=1.68179$) [25, 26]. The matrix of the experimental method is shown in Table 1. Table 2 shows Cu NPs deduced via the electrodeposition process.

Crystalline size of the Cu NP was estimated from Scherer's Equation (1)

TABLE 1: Electrodeposition parameters and their levels.

Electrodeposition parameters	Units	Low value	High value
Concentration of CuSO_4	$\text{g}\cdot\text{l}^{-1}$	4.4	5.6
Distance between the electrodes	cm	3.4	4.6
Potential difference between the electrodes	V	15	24

$$D = \frac{K\lambda}{\beta \cos \theta}, \quad (1)$$

where " λ " = wavelength of X-ray, " β " = full width at half maximum, " θ " = diffraction angle, and " D " = crystalline size.

The interplanar distance was computed by employing Bragg's law Equation (2).

$$n\lambda = 2d \sin \theta. \quad (2)$$

4.2. Modeling for the Size of Cu NPs. The relationship between the input and output was analyzed through a correlation matrix and shown in Table 3. A correlation matrix is a table that summarizes the relationship between multiple variables in a dataset. It shows the correlation coefficients between each pair of variables, which indicate the strength and direction of the linear relationship between them. The values of the correlation coefficient range from -1 to 1 , with 1 indicating a perfect positive correlation, -1 indicating a perfect negative correlation, and 0 indicating no correlation. A correlation matrix is often used in statistical analysis to identify patterns and relationships between variables and to inform the selection of appropriate analytical methods.

The correlation matrix in Table 3 shows the pairwise correlations between four variables: concentration of CuSO_4 , the distance between the electrodes, a potential difference between

TABLE 2: Experimental design matrix.

S. no.	Concentration of CuSO ₄	Distance between the electrodes	Potential difference between the electrodes	Cu NP size (nm)
1	4.4	3.4	15	24.0
2	5	4	19.5	25.0
3	5.6	3.4	15	25.0
4	4.4	4.6	24	24.0
5	6	4	19.5	25.0
6	4.4	3.4	24	25.0
7	5.6	4.6	24	25.0
8	5	4	19.5	24.0
9	4.4	4.6	15	26.0
10	5	4	19.5	23.0
11	5	4	19.5	26.0
12	5	3	19.5	25.0
13	5	4	19.5	25.0
14	5	5	19.5	25.0
15	5	4	19.5	26.0
16	5.6	4.6	15	24.0
17	5.6	3.4	24	27.0
18	5	4	12	25.0
19	4	4	19.5	22.0
20	5	4	27	20.0

TABLE 3: Correlation matrix.

Factors	Concentration of CuSO ₄	Distance between the electrodes	Potential difference between the electrodes	Cu NP size (nm)
Concentration of CuSO ₄	1			
Distance between the electrodes	0	1		
Potential difference between electrodes	0	-2.4E-17	1	
Cu NP size (nm)	0.283579	-0.08102	-0.25657	1

electrodes, and Cu NP size in nanometers. The diagonal of the matrix contains the correlation coefficients between each variable and itself, which are always 1. The off-diagonal elements represent the correlation coefficients between pairs of variables. For example, the coefficient at position (1,4) is 0.283579, which indicates a moderate positive correlation between the concentration of CuSO₄ and Cu NP size. Similarly, the coefficient at position (2,3) is $-2.4E-17$, close to 0, and indicates no correlation between electrode distance and the potential difference between electrodes. Overall, the correlation matrix can provide insights into the relationships between variables and guide further analysis or experimentation.

The architecture of ANN is shown in Figure 6. The application of ANN for predicting and modeling Cu NP mean size depends on network architecture, training algorithms, network type, neural network weight, number of iterations, and momentum rate. A feed forward backpropagation neural network (FFBPNN) with “sigmoid” hidden neurons is an extensively employed neural network (NN) type, and the network is trained with Levenberg–Marquardt backpropagation algorithm (trainlm) [26].

Input data are offered to the input layer of the NN, and the output layer of the NN holds the response of the

input data. The intermediate layer is a hidden layer used to characterize and estimate the relationship between the structure of these networks. Training of NN is effectively performed with a sequence of corresponding input and output data. Every hidden and output neuron treats its inputs by manifold each input data by its related weight and then using a nonlinear transfer function to generate the result. The NN’s learning process changed the neuron weights by continuous iterations in response to the residuals among the actual and target values. The sum of squared error (SSE), regression coefficients (R^2), and mean squared error (MSE) values were used for the evaluation of ANN performance [27]. Table 4 shows the MSE values of training and testing for different hidden layers. Table 4 shows that the hidden layer with ten neurons provides the least MSE error for training and testing.

Weights (W) and biases (b) for all the layers of neurons are integrated with the transfer function to achieve the equation.

- (i) The nodes of three input layers and a first bias node are linked to four hidden layer nodes. There were 12 weights and four biases between the first two layers [25].

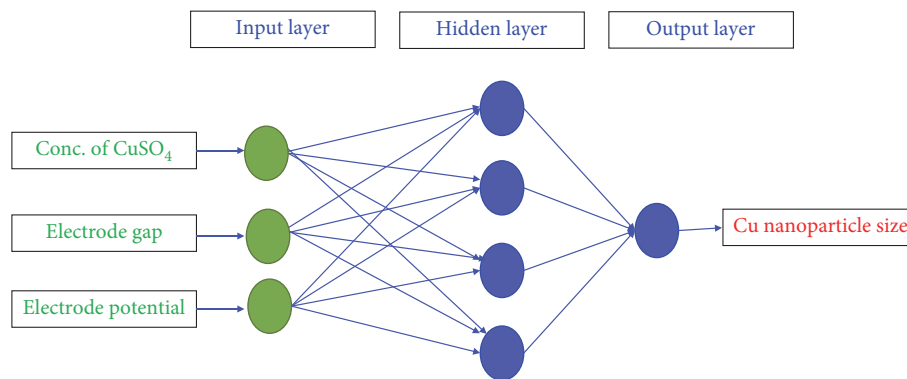


FIGURE 6: Architecture of ANN.

TABLE 4: MSE for various hidden layer.

S. no.	Number of hidden layers	MSE–training error	MSE–testing error	MSE–validation error
1	4	1.53439	1.95534	1.30800
2	5	3.13053e–1	4.19351e–1	4.30695e–1
3	7	3.52380e–1	2.35185e–1	4.00370e–1
4	8	3.8609e–1	3.63864e–1	1.34631e–1
5	10	3.73952e–1	4.81492e–1	7.43702e–2
6	12	2.68907e–1	9.00509e–1	1.31692e–1
7	15	7.50953e–1	1.17548e–1	2.01336e–1

The “tansig” transfer function was selected to compute the weights of 12 inputs ($w_{i,j}$) and four biases (b^l_j).

- (ii) The output (mean size of Cu NPs) is a function of the output transfer function (purelin), which consists of a summation of bias values and weights. The weights have been multiplied by the results obtained from the hidden layer. For every iteration, bias and weight values change to decrease the error.

ANN is utilized for training the electrolysis process parameters by seeing the results shown in Table 2. The dataset was divided into three groups such as 70% of the data for training and 15% for testing, and 15% for validation. The weight between the succeeding layers minimizes the difference between trained and actual values.

With ten neurons in the hidden layer, the performance of different topologies (fitnet and patternnet) with varying transfer functions (Levenberg–Marquardt backpropagation (trainlm), Bayesian regularization backpropagation (trainbr), scaled conjugate gradient backpropagation (trainscg)) is shown in Table 5. The most negligible value of mean absolute error (MAE), MSE, and root-mean-square error (RMSE) and higher values of R -square and VAF (closer to 1) are most desirable for better prediction of the response. Table 5 shows that FFBPNN with Levenberg–Marquardt (trainlm) transfer function with softmax output neurons (patternnet) performed better than other networks in this study. Figure 7 shows the performance of

Levenberg–Marquardt backpropagation (trainlm) with softmax output neurons. The network provides the least MSE of 2.5244e–30 nm in six iterations.

The measured and predicted Cu NP mean size is shown in Figure 8, indicating that the trained network performed reasonably well in prediction [26]. The predicted Cu NP size is very close to the experimental values. Similar results were found in the literature [10, 28].

5. Parameter Optimization Using Nature-Inspired Algorithms

Recently, metaheuristic algorithms have been applied to solve complex real-world problems from numerous fields, like manufacturing, scheduling, planning, and engineering optimization problems. Intensification and diversification are the fundamentals of a metaheuristic algorithm. The right balance between these two is essential to solving a real-world problem effectively. Most metaheuristic algorithms are inspired by biological progression and swarm behavior [22].

5.1. GA. In this study, GA was employed to optimize the electrolysis parameters to identify the mean size of Cu NPs. GA determines optimum operating conditions for the electrolysis parameters and makes Cu NPs with minimum particle size. The regression Equation (3) was obtained from RSM regression analysis and considered an objective function to optimize the electrodeposition parameters.

TABLE 5: Performance of NN with different topologies and transfer functions.

Performance measures/training algorithm	Trainlm with linear output neurons (fitnet)	Trainbr with linear output neurons (fitnet)	Trainscg with linear output neurons (fitnet)	Trainlm with softmax output neurons (patternnet)	Trainbr with linear output neurons (patternnet)	Trainscg with linear output neurons (patternnet)
Mean square error (MSE)	3.73952e-1	9.08727e-1	5.24238e-1	2.5244e-30	6.25453e-19	1.21640e-1
Root mean square error (RMSE)	0.611516	0.953272	0.724043	1.49E-15	7.91E-10	0.348769
Mean absolute error (MAE)	0.11798	0.12765	0.13756	0.0092e-3	0.00256e-5	0.14874
R-square	0.92086	0.91046	0.91038	0.99994	0.98984	0.87564
Variance accounted for (VAF)	0.9215	0.9120	0.9132	0.9815	0.9752	0.8256

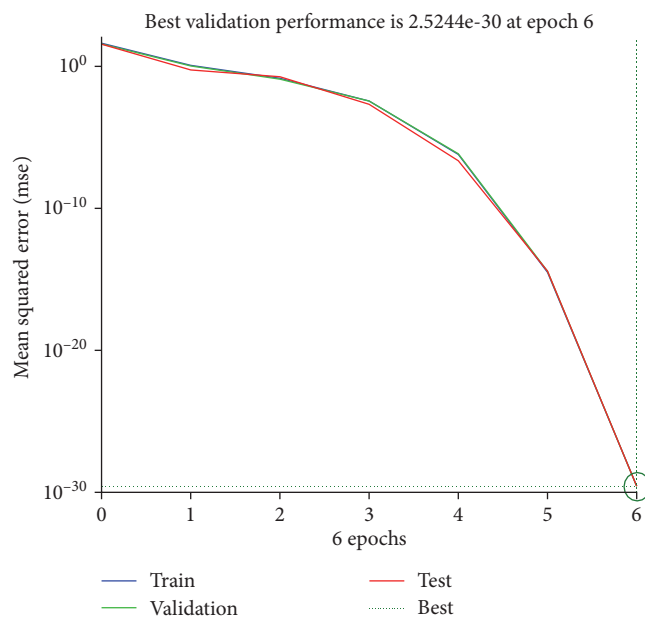


FIGURE 7: Performance of Levenberg–Marquardt backpropagation with softmax output neurons.

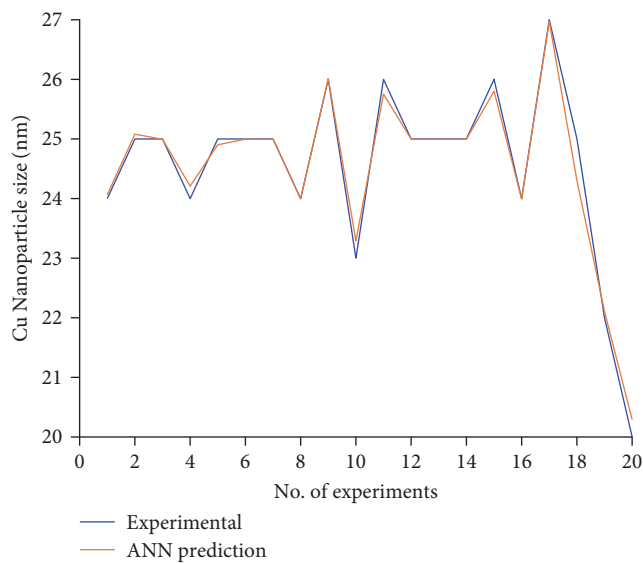


FIGURE 8: Experimental and anticipated values of Cu NPs.

$$\begin{aligned}
 \text{Mean particle size} = & -27.40672 + (9.96726 \times A) \\
 & + (1.48563 \times B) + (2.42318 \times C) \\
 & + (0.60428 \times A \times B) - (0.36325 \times A \times C) \\
 & + (0.013675 B \times C) - (0.47380 \times A^2) \\
 & - (0.47460 \times B^2) - (0.023462 \times C^2).
 \end{aligned} \tag{3}$$

where A = concentration of CuSO_4 , B = electrode distance, and C = electrode potential difference.

The initial parameters considered for GA optimization are listed below:

- (i) Population size = 100
- (ii) Crossover = 0.1
- (iii) Rate of mutation = 0.01
- (iv) Number of generations = 500
- (v) Objective = minimization

The time required to obtain the optimum process parameters was 17 s. The optimum conditions determined by GA for producing the Cu NPs are shown in Table 6.

5.2. FA. The parameters considered for FA are given below:

- (i) Maximum number of iterations = 500
- (ii) Maximum number of fireflies = 20
- (iii) Initial randomness (α_0) = 0.25
- (iv) Randomness factor (α) = 0.90
- (v) Absorption coefficient (γ) = 1
- (vi) Randomness reduction (β) = 0.2
- (vii) Objective = minimization

Equation (3) was used as an objective function. The algorithm was converged within 7 s and gave the optimal parameter. The optimum condition attained from FA is shown in Table 6.

5.3. CS. The parameters employed for the CS algorithm are given below:

- (i) Initial population size = 5
- (ii) Minimum number of eggs = 2
- (iii) Maximum number of eggs = 10

TABLE 6: Optimal electrodeposition parameters obtained from nature-inspired algorithms.

Algorithm	Concentration of electrolyte solution ($\text{g}\cdot\text{l}^{-1}$)	Distance between the electrodes (cm)	Potential difference between the electrodes (V)	Cu NP average size (nm)
GA	4	3	27	22.51
FA	4	3.3	26.8	22.95
CS	4	3	25	21.25
Confirmation test	4	3	27	20.00

(iv) Maximum number of iterations = 500

(v) Number of nests = 50

(vi) Solutions discovery rate = 0.25

The CS algorithm was converged within 8 s, and the optimal parameter was acquired and shown in Table 6.

Table 4 shows the confirmation test with the selected electrodeposition parameters. The mean size of the Cu NPs obtained was 20.00 nm. The particle size is the nominal size used for further applications.

6. Results and Discussion

The key objective is to produce the desired Cu NP size by optimizing electrodeposition parameters. The particle size was estimated through the X-ray diffractometer (XRD) analysis of synthesized Cu NPs. The optimal results were well agreed with experimental results, which led to a smaller particle size of Cu NPs. After optimization, the verification trial was conducted at an electrolyte (CuSO_4) concentration of $4 \text{ g}\cdot\text{l}^{-1}$, the distance between the electrodes of 3 cm, and the potential difference of 27 V. Figure 9 shows the XRD pattern of Cu NPs synthesized from the confirmation trial. Crystalline size of Cu NPs computed from the Debye–Scherer equation was 20 nm which was in line with the size of Cu NPs anticipated through ANN.

An XRD was utilized to record the peaks. An XRD spectrum was recorded from 10° to 90° [29] angles with a step of 0.02° and a scanning rate of $0.05 \text{ deg}\cdot\text{min}^{-1}$. The investigational and usual diffraction angles of Cu NP are shown in Table 7, illustrating that experimental and classic results were almost the same. The crystal structure and phase composition of synthesized Cu NPs are analyzed by XRD, as shown in Figure 9. Based on the XRD data, the synthesized Cu NPs have a face-centered cubic (FCC) crystal structure. The characteristic diffraction peaks (1 1 1), (2 0 0), and (3 1 1) at 2θ values of 37.4° , 43.52° , and 73.71° , respectively, confirm the presence of Cu NPs. Two peak values of 37.4° and 43.52° corresponding to (1 1 1) and (2 0 0) planes were found and evaluated with the Joint Committee on Powder Diffraction Standards, copper file number 03–1,005 [30].

XRD results revealed that synthesized Cu NP has cubic lattices [31]. The XRD results found a gradual reduction in diffraction peaks' intensities. However, the XRD data also show the presence of cuprous oxide (Cu_2O) with diffraction peaks indexed to (1 1 0) and (2 2 0) at 2θ values of 29.1° and 62.9° , respectively. These peaks indicate that partial oxidation of Cu NPs has occurred due to dissolved oxygen in the solution [32, 33]. Therefore, the synthesized Cu NPs are a mixture

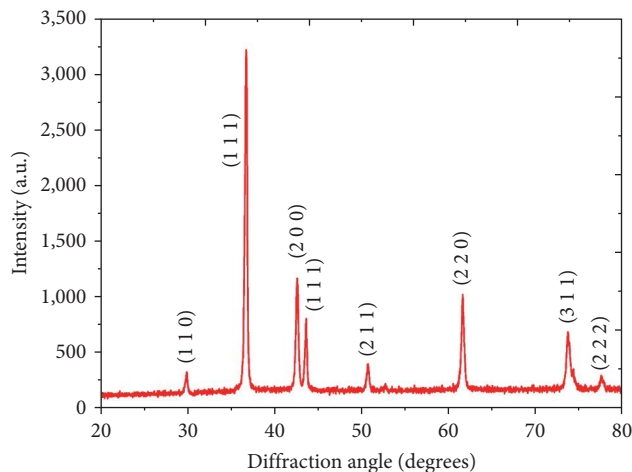


FIGURE 9: XRD pattern of Cu NPs.

TABLE 7: Experimental and standard diffraction values for Cu NP.

Experimentation (2θ)	Standard diffraction (2θ) JCPDS Cu: 03–1,005
43.52°	43.25°
50.65°	50.37°
73.71°	73.99°

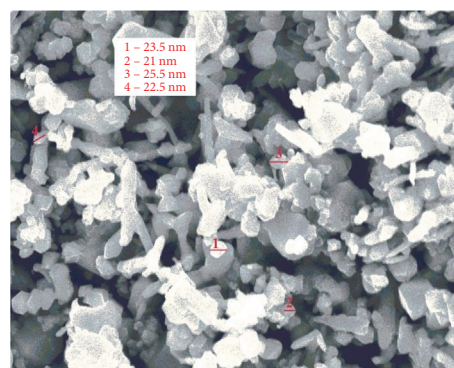


FIGURE 10: SEM image of confirmation trial.

of metallic Cu and Cu_2O phases. The presence of Cu_2O can be undesirable in some applications, but it may also have some beneficial properties, such as catalytic activity.

SEM examination of synthesized Cu NPs at the optimal process parameter is shown in Figure 10. Figure 10 showed that monodisperse hexagonal structure like crystalline Cu NPs was synthesized through electrodeposition. The smaller

NPs yield a higher surface area and improve the catalytic activity. Figure 10 shows the fine particles with hollow sphere fashioned Cu NPs [34]. The fine dispersion of Cu NPs was observed. A reasonable agreement between the particle size was found from SEM and XRD. This can be ascribed to the production of defect-free Cu NPs.

7. Conclusions

Cu NPs were successfully synthesized at an elevated reaction rate and low cost through electrodeposition. It was concluded that the combined approach of ANN and nature-inspired algorithms was used to find the effect of selected electrolysis parameters, namely electrolyte (CuSO_4) concentration, electrode potential difference, and electrode distance on the average size of Cu NP. All the nature-inspired algorithms give similar optimal parameters. The optimum condition for preparing Cu NPs was the concentration of electrolyte solution as $4 \text{ g}\cdot\text{l}^{-1}$, an electrode gap of 3 cm, and the potential difference between electrodes of 27 V. The average particle size obtained from the experimentation was 20 nm. The ANN and nature-inspired algorithms are accurate and give a promising and appropriate way to predict the optimum electrolysis parameters to produce Cu NPs. Trainlm with softmax output neurons (pattern net) network predicts the particle size with an MSE of $2.5244\text{e}-30$.

Data Availability

The data used to support the findings of this study are included in the article.

Conflicts of Interest

The authors declare that they have no conflicts of interest.

References

- [1] C.-Y. Huang and S. R. Sheen, "Synthesis of nanocrystalline and monodispersed copper particles of uniform spherical shape," *Materials Letters*, vol. 30, no. 5-6, pp. 357–361, 1997.
- [2] A. Viswadevarayalu, P. V. Ramana, G. S. Kumar, L. Rathna sylvia, J. Sumalatha, and S. A. Reddy, "Fine ultrasmall copper nanoparticle (UCuNPs) synthesis by using *Terminalia bellirica* fruit extract and its antimicrobial activity," *Journal of Cluster Science*, vol. 27, pp. 155–168, 2016.
- [3] F. Saadati, V. Leghaei, and A. Zamani, "Environmentally benign copper nanoparticles supported on walnut shell as a highly durable nanocatalyst for the synthesis of propargylamines," *Journal of the Serbian Chemical Society*, vol. 82, no. 11, pp. 1211–1221, 2017.
- [4] K. S. Tan and K. Y. Cheong, "Advances of Ag, Cu, and Ag–Cu alloy nanoparticles synthesized via chemical reduction route," *Journal of Nanoparticle Research*, vol. 15, Article ID 1537, 2013.
- [5] A. Tamilvanan, K. Balamurugan, K. Ponappa, and B. M. Kumar, "Copper nanoparticles: synthetic strategies, properties and multifunctional application," *International Journal of Nanoscience*, vol. 13, no. 2, Article ID 1430001, 2014.
- [6] T. Theivasanthi and M. Alagar, "Nano sized copper particles by electrolytic synthesis and characterizations," *International Journal of Physical Sciences*, vol. 6, no. 15, pp. 3662–3671, 2011.
- [7] F. Abbasi-Kesbi, A. M. Rashidi, and B. Astinchap, "Preparation of ultrafine grained copper nanoparticles via immersion deposit method," *Applied Nanoscience*, vol. 8, pp. 221–230, 2018.
- [8] I. M. Dharmadasa and J. Haigh, "Strengths and advantages of electrodeposition as a semiconductor growth technique for applications in macroelectronic devices," *Journal of the Electrochemical Society*, vol. 153, Article ID G47, 2005.
- [9] A. Tamilvanan, M. Bharathiraja, K. Balamurugan, and C. Sasikumar, "Effect of aluminium oxide nanoadditive on diesel along with gasoline fumigation in single cylinder diesel engine," *Journal of Engineering Research*, vol. 10, no. 3B, pp. 145–155, 2022.
- [10] V. K. Deshmukh, M. Pradhan, H. Narang, M. S. Rajput, and S. K. Mukti, "Prediction of electrodeposited copper ions in high speed jet electrodeposition for MEMS fabrication using ANN," *Materials Today: Proceedings*, vol. 28, Part 4, pp. 2527–2531, 2020.
- [11] M. B. Kale, R. A. Borse, A. G. A. Mohamed, and Y. Wang, "Electrocatalysts by electrodeposition: recent advances, synthesis methods, and applications in energy conversion," *Advanced Functional Materials*, vol. 31, no. 25, Article ID 2101313, 2021.
- [12] J. Xue, Q. Wu, Z. Wang, and S. Yi, "Function of additives in electrolytic preparation of copper powder," *Hydrometallurgy*, vol. 82, no. 3-4, pp. 154–156, 2006.
- [13] R. K. Nekouie, F. Rashchi, and N. N. Joda, "Effect of organic additives on synthesis of copper nano powders by pulsing electrolysis," *Powder Technology*, vol. 237, pp. 554–561, 2013.
- [14] S. Sarfraz, A. T. Garcia-Esparza, A. Jedidi, L. Cavallo, and K. Takanabe, "Cu–Sn bimetallic catalyst for selective aqueous electroreduction of CO_2 to CO," *ACS Catalysis*, vol. 6, no. 5, pp. 2842–2851, 2016.
- [15] M. T. Crespo, "A review of electrodeposition methods for the preparation of alpha-radiation sources," *Applied Radiation and Isotopes*, vol. 70, no. 1, pp. 210–215, 2012.
- [16] J. Tang and K. Azumi, "Optimization of pulsed electrodeposition of aluminum from AlCl_3 -1-ethyl-3-methylimidazolium chloride ionic liquid," *Electrochimica Acta*, vol. 56, no. 3, pp. 1130–1137, 2011.
- [17] B. Li, Y. Chen, L. Yan, and J. Ma, "Pulse current electrodeposition of Al from an AlCl_3 -EMIC ionic liquid containing NdCl_3 ," *Electrochemistry*, vol. 78, no. 6, pp. 523–525, 2010.
- [18] N. Saha, G. Astray, and S. D. Gupta, "Modelling and optimization of biogenic synthesis of gold nanoparticles from leaf extract of *Swertia chirata* using artificial neural network," *Journal of Cluster Science*, vol. 29, pp. 1151–1159, 2018.
- [19] J. Gokulachandran and R. Padmanaban, "Prediction of remaining useful life of cutting tools: a comparative study using soft computing methods," *International Journal of Process Management and Benchmarking*, vol. 8, no. 2, pp. 156–181, 2018.
- [20] M. Dehestani, G. R. Khayati, and S. Sharafi, "An improved optimization model to predict the microhardness of Ni/ Al_2O_3 nanocomposite coatings prepared by electrodeposition: a hybrid artificial neural network-modified particle swarm optimization approach," *Measurement*, vol. 179, Article ID 109423, 2021.
- [21] S. Kumar, A. K. Gupta, P. Chandna, G. Bhushan, and A. Kumar, "A novel approach of GEF and GA for the optimization of multi-objective wire EDM process during the

- machining of DC53 super alloy,” *Proceedings of the Institution of Mechanical Engineers, Part E: Journal of Process Mechanical Engineering*, vol. 235, no. 4, pp. 1119–1131, 2021.
- [22] S. Katoch, S. S. Chauhan, and V. Kumar, “A review on genetic algorithm: past, present, and future,” *Multimedia Tools and Applications*, vol. 80, pp. 8091–8126, 2021.
- [23] V. Kumar and D. Kumar, “A systematic review on firefly algorithm: past, present, and future,” *Archives of Computational Methods in Engineering*, vol. 28, pp. 3269–3291, 2021.
- [24] X.-S. Yang, *Nature-Inspired Optimization Algorithms*, Elsevier, 2014.
- [25] S. Shankar, T. Mohanraj, and A. Pramanik, “Tool condition monitoring while using vegetable based cutting fluids during milling of inconel 625,” *Journal of Advanced Manufacturing Systems*, vol. 18, no. 4, pp. 563–581, 2019.
- [26] S. Shankar, T. Mohanraj, and R. Rajasekar, “Prediction of cutting tool wear during milling process using artificial intelligence techniques,” *International Journal of Computer Integrated Manufacturing*, vol. 32, no. 2, pp. 174–182, 2019.
- [27] G. A. Ramaswamy, A. Krishna, M. Gautham, S. S. Sudharshan, and J. Gokulachandran, “Optimisation and prediction of machining parameters in EDM for Al-ZrO₂ using soft computing techniques with Taguchi method,” *International Journal of Process Management and Benchmarking*, vol. 11, no. 6, pp. 864–890, 2021.
- [28] M. Fan, J. Hu, R. Cao, K. Xiong, and X. Wei, “Modeling and prediction of copper removal from aqueous solutions by nZVI/rGO magnetic nanocomposites using ANN-GA and ANN-PSO,” *Scientific Reports*, vol. 7, Article ID 18040, 2017.
- [29] S. Ramesh, S. Vetrivel, P. Suresh, and V. Kaviarasan, “Characterization techniques for nano particles: a practical top down approach to synthesize copper nano particles from copper chips and determination of its effect on planes,” *Materials Today: Proceedings*, vol. 33, Part 7, pp. 2626–2630, 2020.
- [30] P. Bindu and S. Thomas, “Estimation of lattice strain in ZnO nanoparticles: X-ray peak profile analysis,” *Journal of Theoretical and Applied Physics*, vol. 8, pp. 123–134, 2014.
- [31] R. Mittu, “Synthesis, characterization of copper nanoparticles—a review,” *International Advanced Research Journal in Science, Engineering and Technology*, vol. 3, no. 5, pp. 37–40, 2016.
- [32] G. Mishra, S. K. Verma, D. Singh, P. K. Yadawa, and R. R. Yadav, “Synthesis and ultrasonic characterization of Cu/PVP nanoparticles-polymer suspensions,” *Open Journal of Acoustics*, vol. 1, no. 1, pp. 9–14, 2011.
- [33] A. D. Karthik and K. Geetha, “Synthesis of copper precursor, copper and its oxide nanoparticles by green chemical reduction method and its antimicrobial activity,” *Journal of Applied Pharmaceutical Science*, vol. 3, no. 5, pp. 16–21, 2013.
- [34] B. G. Mahmoud, M. Khairy, F. A. Rashwan, C. W. Foster, and C. E. Banks, “Self-assembly of porous copper oxide hierarchical nanostructures for selective determinations of glucose and ascorbic acid,” *RSC Advances*, vol. 6, no. 18, pp. 14474–14482, 2016.